

Multi-Static ISAC in Cell-Free Massive MIMO: Precoder Design and Privacy Assessment

Isabella W. G. da Silva, Diana P. M. Osorio, and Markku Juntti

Centre for Wireless Communications, University of Oulu, P.O.Box 4500, FI-90014, Finland

Emails: {isabella.dasilva, diana.moyaosorio, markku.juntti}@oulu.fi

Abstract—A multi-static sensing-centric integrated sensing and communication (ISAC) network can take advantage of the cell-free massive multiple-input multiple-output infrastructure to achieve remarkable diversity gains and reduced power consumption. While the conciliation of sensing and communication requirements is still a challenge, the privacy of the sensing information is a growing concern that should be seriously taken on the design of these systems to prevent other attacks. This paper tackles this issue by assessing the probability of an internal adversary to infer the target location information from the received signal by considering the design of transmit precoders that jointly optimizes the sensing and communication requirements in a multi-static-based cell-free ISAC network. Our results show that the multi-static setting facilitates a more precise estimation of the location of the target than the mono-static implementation.

Index Terms—cell-free massive MIMO, ISAC, multi-static sensing, precoder design, privacy.

I. INTRODUCTION

The sixth generation (6G) of wireless communications is expected to heavily influence every aspect of the Society of 2030. Several applications envisioned for 6G will be supported by sensing capabilities, with the network acting as a sensor. For this becoming reality, the new paradigm of integrated sensing and communications (ISAC) plays an important role by allowing an intelligent share of wireless resources and the support for a number of use cases such as autonomous vehicles and smart homes [1].

So far, the research on ISAC systems has mainly focused on mono-static sensing. However, the employment of mono-static sensing requires the co-located sensing transmitter and receiver to be full-duplex. Hence, multi-static sensing ISAC systems, in which there are multiple non-co-located transmitters and receivers for sensing, can provide diversity gain while avoiding the need for full-duplex nodes [2]. For instance, in [2], Behdad *et al.* assessed the probability of detection of a single target in a cell-free massive multiple-input multiple-output MIMO ISAC system where a number of ISAC transmitters and sensing receivers are deployed to detect the target and to transmit data to multiple communication users (UEs). Moreover, in [3], Huang *et al.* proposed a coordinated power control design for a networked ISAC system aiming to maximize the signal-to-interference-plus-noise ratio (SINR) at the UEs and maximize the Crámer-Rao lower bound (CRLB) of the target location estimate. Both works demonstrated that, in comparison to communication-

centric designs, a cell-free massive MIMO ISAC design requires less transmit power to attain more accurate detection.

Nevertheless, the design of joint precoders for sensing and communications employed in most of works with mono-static or multi-static ISAC systems considered the simultaneous transmission of individual radar and communication waveforms [4], [5]. Thus, the transmit precoder contains information about the target location and the data intended for the UEs. Indeed, the advancements on ISAC design have exacerbated security and privacy concerns since the communication information could be exposed to untrusted targets, and malicious UEs could try to infer the position of targets. In this sense, security and privacy aspects have recently started to emerge as a crucial part for the design of ISAC. For instance, the works in [6], [7] and [8] have focused on the design of beamformers with secrecy requirements to prevent untrusted targets from eavesdropping information from UEs. In [6], Su *et al.* proposed a beamforming design to minimize the signal-to-noise ratio (SNR) at a potential malicious target constrained to minimal SINR requirements for the UEs. In [7], the transmit beamforming is obtained via a weighted optimization between radar estimation CRLB and the communication secrecy rate. Also, in [8], Ren *et al.* proposed a beamforming design to minimize the beam pattern matching error constrained to secrecy rates requirements in a network with multiple targets, with some of them assumed as malicious.

On the other hand, the privacy of the sensing information remains barely explored while being an important source of concern as it can trigger further attacks. In our earlier work [9], we addressed this aspect by evaluating the capability that an internal adversary of the network will have to infer the angular position of a target by an UE that acts as an adversary. Results demonstrated that if the adversary is capable to infer the transmit precoder, the detection surpasses fifty percent of the cases, which entails a serious privacy breach for ISAC systems.

Accordingly, recognizing the benefits of multi-static sensing and the seriousness of possible privacy leakages in ISAC systems, in this work we investigate a multi-static sensing-centric ISAC network in a cell-free massive MIMO scenario, with multiple MIMO UEs and a point-like target. In this scenario, one of the UEs acts maliciously by trying to estimate the position of the target from the observations of the received signal. The main contributions of this work

are as follows: i) we propose a transmit precoder design to maximize the sensing SINR constrained to a minimal SINR for the UEs and a transmit power limit requirement; ii) a replica of the transmit beampattern from each transmitter access point (AP) is computed based on an expectation-maximization (EM) approach.

II. SYSTEM MODEL

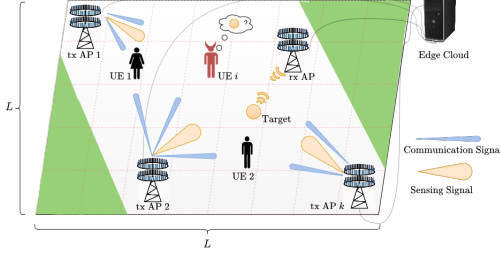


Fig. 1: System Model

Consider the ISAC system as illustrated in Fig. 1, where N_{Tx} APs are jointly serving N_{Ue} UEs equipped with M_{Ue} antennas, while also detecting a point-like target. In this system, one of the UEs acts as an adversary and intends to discover the location of the target. The other N_{Rx} APs are acting as sensing receivers that simultaneously sense the location of the target. The transmit and receive APs are equipped with M_{AP} half-wavelength-spaced isotropic antennas deployed as a uniform linear array (ULA). It is further assumed that all APs are connected to the edge cloud, where the processing is done in a centralized manner, and are fully synchronized. Similar to [2], we assume that the transmitted signal by the k th transmit AP is given by a weighted sum of communication symbols and sensing signals. Hence, at time instance n , the transmitted signal $\mathbf{x}_k[n] \in \mathbb{C}^{M_{AP}}$ can be written as

$$\mathbf{x}_k[n] = \sum_{i=1}^{N_{Ue}} \mathbf{w}_{i,k} s_i[n] + \mathbf{w}_{t,k} s_t[n] = \mathbf{W}_k \mathbf{s}[n], \quad n = 0, \dots, N-1, k = 1, \dots, N_{Tx}, \quad (1)$$

where $\mathbf{s}[n] = [s_1[n], \dots, s_{N_{Ue}}[n], s_t[n]]^T$ is the $(N_{Ue} + 1) \times 1$ vector containing the $N_{Ue} \times 1$ parallel communications symbols intended to the N_{Ue} users plus the sensing signal, which is independent of the UE's data signals. Also, $\mathbf{w}_{i,k}$ and $\mathbf{w}_{t,k}$ are the $M_{AP} \times 1$ transmit precoder vector of the k th transmitter AP for the i th user and for the sensing of the target, respectively. In addition, the users are assumed to employ a receive beamformer \mathbf{u}_i , with size $M_{Ue} \times 1$, to estimate the transmitted data stream. Accordingly, the estimated data stream at the i th user at time n is given by

$$y_i[n] = \mathbf{u}_i^H \left(\sum_{k=1}^{N_{Tx}} \mathbf{H}_{i,k} \mathbf{W}_k \mathbf{s}[n] + \mathbf{n}_i[n] \right), \quad (2)$$

where $\mathbf{H}_{i,k}$ is the $M_{Ue} \times M_{AP}$ channel coefficient matrix between the k th AP and UE i . It is assumed that there is no dominant line-of-sight (LOS) component between APs and UEs, so $\mathbf{H}_{i,k}$, undergoes Rayleigh block fading, for all

$i \in 1, \dots, N_{Ue}$. Moreover, \mathbf{n}_i is the noise component at the i th user, modeled as signal-independent, zero-mean, additive white Gaussian noise (AWGN) with variance $\sigma_i^2 \mathbf{I}$. Following, the SINR at UE i given the transmission of AP k is written as

$$\gamma_{i,k} = \frac{|\mathbf{u}_i^H \mathbf{H}_{i,k} \mathbf{w}_{i,k}|^2}{\sum_{l=1, l \neq i}^{N_{Ue}} |\mathbf{u}_i^H \mathbf{H}_{i,k} \mathbf{w}_{l,k}|^2 + |\mathbf{u}_i^H \mathbf{H}_{i,k} \mathbf{w}_{t,k}|^2 + \sigma_i^2 \|\mathbf{u}_i\|^2}. \quad (3)$$

On the other hand, the signal received by the r th receiver AP at the time instant n is written as

$$\mathbf{y}_r[n] = \sum_{k=1}^{N_{Tx}} \alpha_{r,k} \sqrt{\beta_{r,k}} \mathbf{a}(\phi_r) \mathbf{a}^T(\phi_k) \mathbf{x}_k[n] + \mathbf{n}_r[n], \quad (4)$$

where $\alpha_{r,k}$ is the bi-static unknown radar cross section (RCS) of the target through the reflection path from transmitter AP k to the receiver AP r . Herein, as in [2], it is assumed that the RCS follows the Swerling-I model, so that $\alpha_{r,k}$ is constant throughout a collection of consecutive sensing signals and follows the distribution $\alpha_{r,k} \sim \mathcal{CN}(0, \sigma_{r,k}^2)$. Also, ϕ_i is the azimuth angle from the target position to the i th AP, with $i \in \{k = 1, \dots, N_{Tx}, r = 1, \dots, N_{Rx}\}$. Accordingly, $\mathbf{a}(\phi) \in \mathbb{C}^{M_{AP}}$ is the antenna array steering vector, given by

$$\mathbf{a}(\phi) = [1, e^{j\pi \sin(\phi)}, \dots, e^{j(M_{AP}-1)\pi \sin(\phi)}]^T. \quad (5)$$

Finally, $\mathbf{n}_r[n] \sim \mathcal{CN}(\mathbf{0}, \sigma_n^2 \mathbf{I}_{M_{AP}})$ is the noise component at the r th receiver AP, and $\beta_{r,k}$ is the channel gain of the path between the k th transmitter AP to the target and from the target to the r th receiver AP, which can be calculated as [2]

$$\beta_{r,k} = \frac{\lambda_c^2}{(4\pi)^3 d_{t,k}^2 d_{t,r}^2}, \quad (6)$$

where λ_c is the carrier wavelength, and $d_{t,i}$ is the distance between the target location and the AP i , with $i \in \{k = 1, \dots, N_{Tx}, r = 1, \dots, N_{Rx}\}$. Moreover, the possible clutter caused by permanent or temporary objects is neglected. Accordingly, the sensing SINR, γ_t , is given by

$$\gamma_t = \zeta \left(\sum_{n=1}^{N-1} \mathbf{s}^H[n] \left(\sum_{r=1}^{N_{Rx}} \sum_{k=1}^{N_{Tx}} \sum_{j=1}^{N_{Tx}} \varphi_{r,k,j} \mathbf{W}_k^H \mathbf{A}_{k,j} \mathbf{W}_j \right) \mathbf{s}[n] \right), \quad (7)$$

with $\varphi_{r,k,j} = \sqrt{\beta_{r,k} \beta_{r,j}} \mathbf{a}^H(\phi_r) \text{cov}(\alpha_{r,j}, \alpha_{r,k}) \mathbf{a}(\phi_r)$, $\mathbf{A}_{k,j} = \mathbf{a}^*(\phi_k) \mathbf{a}^T(\phi_j)$, and $\zeta = 1/(N-1)M_{AP}N_{Rx}\sigma_n^2$.

III. PRECODER DESIGN

For the design of the ISAC transmit precoding, the goal is to maximize the sensing SINR in (7) under transmit power and communication quality of service (QoS) constraints, which can be formulated as

$$\mathcal{P}: \max_{\mathbf{W}, \mathbf{u}} \gamma_t \quad (8a)$$

$$\text{s. t. } \gamma_{i,k} \geq \Gamma, i = 1, \dots, N_{Ue}, k = 1, \dots, N_{Tx} \quad (8b)$$

$$\sum_{i=1}^{N_{Ue}} \|\mathbf{w}_{i,k}\|^2 + \|\mathbf{w}_{t,k}\|^2 \leq P_T, k = 1, \dots, N_{Tx}, \quad (8c)$$

where Γ is the communication SINR threshold, and P_T is the transmit power limit for the transmitter APs. To solve \mathcal{P} , an iterative process is employed. At first, the UEs receive beamformers \mathbf{u}_i , $i=1, \dots, N_{\text{Ue}}$ are randomly chosen and fixed. Nonetheless, note that the optimization problem in \mathcal{P} is still not convex due to the non-concave objective function and non-convex constraint in (8b). To handle this, (8a) can be split into two sub-problems as

$$\mathcal{P}1: \max_{\mathbf{W}} \zeta \left(\sum_{n=1}^{N-1} \mathbf{s}^H[n] \left(\sum_{r=1}^{N_{\text{Rx}}} \sum_{k=1}^{N_{\text{Tx}}} \varphi_{r,k,k} \mathbf{W}_k^H \mathbf{A}_{k,k} \mathbf{W}_k \right) \mathbf{s}[n] \right) \quad (9a)$$

s. t. (8b), (8c),

and,

$$\mathcal{P}2: \max_{\mathbf{W}} \zeta \left(\sum_{n=1}^{N-1} \mathbf{s}^H[n] \left(\sum_{r=1}^{N_{\text{Rx}}} \sum_{k=1}^{N_{\text{Tx}}} \sum_{j=1}^{N_{\text{Tx}}} \varphi_{r,k,j} \mathbf{W}_k^H \mathbf{A}_{k,j} \mathbf{W}_j \right) \mathbf{s}[n] \right) \quad (10a)$$

s. t. (8b), (8c).

Next, as in [10], we consider the first-order Taylor approximation to linearize (9a) and (8b), and employ the constrained convex-concave procedure (CCCP) to iteratively solve the approximated convex problem until a convergence criterion is attained. Thus, at the p th iteration, $\mathcal{P}1$ is solved as

$$\mathcal{P}1': \max_{\mathbf{W}, \tau_{i,k}, \mu_{i,k}} \zeta \left(\sum_{n=1}^{N-1} \mathbf{s}^H[n] \left(\sum_{r=1}^{N_{\text{Rx}}} \sum_{k=1}^{N_{\text{Tx}}} \varphi_{r,k,k} \left(2 \left[\mathbf{W}_k^{(p-1)} \right]^H \mathbf{A}_{k,k} \times \left(\mathbf{W}_k - \mathbf{W}_k^{(p-1)} \right) + \left[\mathbf{W}_k^{(p-1)} \right]^H \mathbf{A}_{k,k} \mathbf{W}_k^{(p-1)} \right) \right) \mathbf{s}[n] \right) \quad (11a)$$

$$\text{s. t. } |\mathbf{u}_i^H \mathbf{H}_{i,k} \mathbf{w}_{i,k}^{(p-1)}|^2 + 2 \left[\mathbf{w}_{i,k}^{(p-1)} \right]^H \mathbf{H}_{i,k}^H \mathbf{u}_i \mathbf{u}_i^H \mathbf{H}_{i,k} \times \left(\mathbf{w}_{i,k} - \mathbf{w}_{i,k}^{(p-1)} \right) \geq \tau_{i,k}, \forall i, \forall k \quad (11b)$$

$$\sum_{l=1}^{N_{\text{Ue}}} |\mathbf{u}_i^H \mathbf{H}_{i,k} \mathbf{w}_{l,k}|^2 + |\mathbf{u}_i^H \mathbf{H}_{i,k} \mathbf{w}_{t,k}|^2 + \sigma_i^2 \|\mathbf{u}_i\|^2 \leq \mu_{i,k} \quad (11c)$$

$$\tau_{i,k} \geq \Gamma \mu_{i,k}, \forall i, \forall k, \quad (8c), \quad (11d)$$

where τ and μ are slack variables. $\mathcal{P}1'$ is a concave problem. $\mathcal{P}2$, on the other hand, is approximated to the following

$$\mathcal{P}2': \max_{\mathbf{W}, \tau_{i,k}, \mu_{i,k}} \zeta \left(\sum_{n=1}^{N-1} \mathbf{s}^H[n] \left(\sum_{r=1}^{N_{\text{Rx}}} \sum_{k=1}^{N_{\text{Tx}}} \sum_{j=1}^{N_{\text{Tx}}} \varphi_{r,k,j} \mathbf{W}_k^H \mathbf{A}_{k,j} \times \mathbf{W}_j^{(p-1)} \right) \mathbf{s}[n] \right) \quad (12a)$$

s. t. (11b), (11c), (11d), (8c).

which is a concave problem. Accordingly, both optimization can be solved with convex toolboxes such as CVX. After obtaining the optimal p th \mathbf{W}^* , given by the summation of

the solutions of $\mathcal{P}1'$ and $\mathcal{P}2'$, the transmit precoder matrices are fixed and, for all i , \mathbf{u}_i is updated via the MMSE receiver as [11]

$$\mathbf{u}_i = \sum_{k=1}^{N_{\text{Tx}}} \left(\mathbf{H}_{i,k} \left(\sum_{l=1}^{N_{\text{Ue}}} \mathbf{w}_{l,k} \mathbf{w}_{l,k}^H \right) \mathbf{H}_{i,k}^H + \sigma_i^2 \mathbf{I}_{M_{\text{Ue}}} \right)^{-1} \mathbf{H}_{i,k} \mathbf{w}_{i,k}. \quad (13)$$

Accordingly, the algorithm to obtain the transmit and receive precoders is summarized in Algorithm 1.

Algorithm 1 Precoders Iterative Algorithm

- 1: Choose error tolerances ϵ , maximum number of iterations p_{\max} , and feasible initial points $\mathbf{W}^{(0)}$, and $\mathbf{u}_i(0) \forall i$.
 - 2: $p \leftarrow 0$
 - 3: **repeat**
 - 4: Solve (11a) and (12a) to obtain $\mathbf{W}^{*(p)}$ using $\mathbf{W}^{*(p-1)}$ and $\mathbf{u}_i^{(p-1)}$ from the previous iteration.
 - 5: Solve (13) using $\mathbf{W}^{*(p)}$ to attain $\mathbf{u}_i^{(p)}$.
 - 6: $p++$
 - 7: **until** $\frac{\|\mathbf{W}^{*(p)} - \mathbf{W}^{*(p-1)}\|}{\mathbf{W}^{*(p)}} \leq \epsilon$ and $\frac{\|\mathbf{u}_i^{*(p)} - \mathbf{u}_i^{*(p-1)}\|}{\mathbf{u}_i^{*(p)}} \leq \epsilon$ or $p \geq p_{\max}$
 - 8: **return** \mathbf{W}^* , $\mathbf{u}_i^* \forall i$.
-

IV. ADVERSARY MODEL

Assuming that the UEs know that there is a present target in the network, one of them may act as an adversary. Given its received signal, the UE could try to infer the position of the target by recreating a replica of the transmit beampattern created by the transmitter APs given by

$$\mathbf{B}_k = \mathbf{a}^H(\theta_z) \mathbf{R}_{\mathbf{x}_k} \mathbf{a}(\theta_z), \forall k, \quad (14)$$

where $\{\theta_z\}_{z=1}^Z$ are sampled angle grids, and $\mathbf{R}_{\mathbf{x}_k} = \mathbf{x}_k \mathbf{x}_k^H$ is the covariance matrix of the transmitted signal. To accomplish this, it is considered that the adversary has knowledge of its receive beamforming vector. Also, it is feasible to assume that the adversary knows the position of the N_{Tx} transmitter APs and can create a search area based on that information. Under these considerations, the adversary estimation process starts with the inference of the interference signal from its received signal, which is expressed as(2), is equal to

$$\tilde{\mathbf{y}}_{a,k} = \mathbf{H}_{a,k} \underbrace{\left(\sum_{l=1}^{N_{\text{Ue}}} \mathbf{w}_{l,k} s_l[n] + \mathbf{w}_{t,k} s_t[n] \right)}_{\tilde{\mathbf{x}}_k} + \mathbf{n}_a. \quad (15)$$

We further assume that the real $\mathbf{H}_{a,k}$ is not available at the adversary, but can be calculated as $\mathbf{H}_{a,k} = \hat{\mathbf{H}}_{a,k} + \varepsilon$, where $\hat{\mathbf{H}}_{a,k}$ is the channel estimate, which can be attained via least square estimation with pilot signals as

$$\hat{\mathbf{H}}_{a,k} = \mathbf{y}_{a,k} \mathbf{x}_k^H (\mathbf{x}_k \mathbf{x}_k^H)^{-1}, \quad (16)$$

and ε represents the channel estimation error, modeled as $\mathcal{N}(0, \sigma_\varepsilon^2 \mathbf{I})$. Thus, $\mathbf{H}_{a,k} \sim \mathcal{N}(\hat{\mathbf{H}}_{a,k}, \sigma_\varepsilon^2 \mathbf{I})$.

Then, considering $\tilde{\mathbf{y}}_{a,k}$ as an observable variable, $\mathbf{H}_{a,k}$ as a latent variable, and $\tilde{\mathbf{x}}_k$ as the unknown parameter, an

iterative method to compute the maximum log-likelihood as the EM can be employed to estimate $\tilde{\mathbf{x}}_k$. The EM algorithm is a general technique used to find the maximum likelihood estimates of parameters when part of the data is missing or for latent variable models. The algorithm is divided in two steps, the E-step and the M-step. In the former, the expected value of the log-likelihood function is computed, as well as a current estimate of the unknown parameter. In the latter, the unknown parameter is attained from the maximization of the previously obtained expected value [12].

A. Expectation-Maximization Algorithm

As the goal is to maximize the log-likelihood function, we start by defining it as

$$\mathcal{L} = \log(p_{\tilde{\mathbf{y}}_{a,k}}(\tilde{\mathbf{x}}_k)) = \log\left(\int p_{\tilde{\mathbf{y}}_{a,k}, \mathbf{H}_{a,k}}(\tilde{\mathbf{x}}_k) d\mathbf{H}_{a,k}\right), \quad (17)$$

where $p_{\tilde{\mathbf{y}}_{a,k}}$ is the probability density function (PDF) of the variable $\tilde{\mathbf{y}}_{a,k}$, and $p_{\tilde{\mathbf{y}}_{a,k}, \mathbf{H}_{a,k}}(\tilde{\mathbf{x}}_k)$ stands for the joint PDF of $\mathbf{y}_{a,k}$ and $\mathbf{H}_{a,k}$, and can be rewritten as

$$p_{\tilde{\mathbf{y}}_{a,k}, \mathbf{H}_{a,k}}(\tilde{\mathbf{x}}_k) = p_{\mathbf{H}_{a,k}}(\mathbf{H}_{a,k}) p_{\tilde{\mathbf{y}}_{a,k} | \mathbf{H}_{a,k}}(\tilde{\mathbf{x}}_k), \quad (18)$$

where $p_{\tilde{\mathbf{y}}_{a,k} | \mathbf{H}_{a,k}}(\tilde{\mathbf{x}}_k)$ is the conditional pdf of $\tilde{\mathbf{y}}_{a,k}$ and $\mathbf{H}_{a,k}$. As in [13], to overcome the sensitivity of the Gaussian distribution to outliers, the heavy-tailed Student's t distribution is considered to describe $p_{\tilde{\mathbf{y}}_{a,k} | \mathbf{H}_{a,k}}(\tilde{\mathbf{x}}_k)$, that is,

$$p_{\tilde{\mathbf{y}}_{a,k} | \mathbf{H}_{a,k}}(\tilde{\mathbf{x}}_k) \sim \text{lst}(\mathbf{H}_{a,k} \tilde{\mathbf{x}}_k, \sigma_a^2 \mathbf{I}, v), \\ = \int_0^\infty \mathcal{N}\left(\mathbf{H}_{a,k} \tilde{\mathbf{x}}_k, \frac{\sigma_a^2 \mathbf{I}}{u}\right) \mathcal{G}\left(\frac{v}{2}, \frac{v}{2}\right) du, \quad (19)$$

where v is the degree of freedom, u is an auxiliary hidden variable, and \mathcal{G} is the gamma function. Thus, the latent variable is redefined as $\mathbf{h}_{a,k} = \{\mathbf{H}_{a,k}, u\}$, and the model parameters are given by $\vartheta = \{\tilde{\mathbf{x}}_k, v\}$. Next, based on [12], by introducing an arbitrary distribution $q(\mathbf{h}_{a,k})$ over the latent variable $\mathbf{h}_{a,k}$, \mathcal{L} can be decomposed in two terms as

$$\mathcal{L} = \int q(\mathbf{h}_{a,k}) \log(p_{\tilde{\mathbf{y}}_{a,k}, \mathbf{h}_{a,k}}(\vartheta)) d\mathbf{h}_{a,k}, \\ = \int q(\mathbf{h}_{a,k}) \log\left(\frac{p_{\tilde{\mathbf{y}}_{a,k}, \mathbf{h}_{a,k}}(\vartheta)}{q(\mathbf{h}_{a,k})} \frac{q(\mathbf{h}_{a,k})}{p_{\mathbf{h}_{a,k} | \tilde{\mathbf{y}}_{a,k}}(\vartheta)}\right) d\mathbf{h}_{a,k}, \\ = \underbrace{\int q(\mathbf{h}_{a,k}) \log\left(\frac{p_{\tilde{\mathbf{y}}_{a,k}, \mathbf{h}_{a,k}}(\vartheta)}{q(\mathbf{h}_{a,k})}\right) d\mathbf{h}_{a,k}}_{\mathcal{F}_{\tilde{\mathbf{y}}_{a,k}}(q, \vartheta)} + \text{KLD}, \quad (20)$$

where KLD is given by

$$\text{KLD} = \int q(\mathbf{h}_{a,k}) \log\left(\frac{q(\mathbf{h}_{a,k})}{p_{\mathbf{h}_{a,k} | \tilde{\mathbf{y}}_{a,k}}(\vartheta)}\right) d\mathbf{h}_{a,k}, \quad (21)$$

which is the Kullback-Leiber divergence, and has the property of always being greater or equal to zero. Hence, the E-step and the M-step of the EM algorithm can be described only in terms of $\mathcal{F}_{\tilde{\mathbf{y}}_{a,k}}(q, \vartheta)$ as presented next.

1) *E-step*: \mathcal{F} is maximized in terms of $q(\mathbf{h}_{a,k})$ for a fixed ϑ . Thus, after every $(a+1)$ th iteration, $q(\mathbf{h}_{a,k})$ is updated as

$$q^{a+1}(\mathbf{h}_{a,k}) = \arg \max_{q(\mathbf{h}_{a,k})} \mathcal{F}_{\tilde{\mathbf{y}}_{a,k}}(q, \vartheta^a). \quad (22)$$

Given that $\mathbf{H}_{a,k}$ and u are independent, q can be factorized as $q(\mathbf{h}_{a,k}) = q(\mathbf{H}_{a,k})q(u)$. And based on [13], $q(\mathbf{H}_{a,k})$ and $q(u)$ are optimal as

$$q(\mathbf{H}_{a,k}) \propto p_{\mathbf{H}_{a,k}}(\mathbf{H}_{a,k}) \exp\left\{\mathbb{E}_u\left[\log \mathcal{N}\left(\mathbf{H}_{a,k} \tilde{\mathbf{x}}_k, \frac{\sigma_a^2 \mathbf{I}}{u}\right)\right]\right\}, \quad (23)$$

$$q(u) \propto \mathcal{G}\left(\frac{v}{2}, \frac{v}{2}\right) \exp\left\{\mathbb{E}_{\mathbf{H}_{a,k}}\left[\log \mathcal{N}\left(\mathbf{H}_{a,k} \tilde{\mathbf{x}}_k, \frac{\sigma_a^2 \mathbf{I}}{u}\right)\right]\right\}. \quad (24)$$

Accordingly, the distribution in (23) have the mean and covariance given, respectively, by

$$\mathbb{E}_{\mathbf{H}_{a,k}}[q(\mathbf{H}_{a,k})] = \left[\mathbf{\Omega}_{\mathbf{H}} \left(\frac{1}{\sigma_\epsilon^2} \hat{\mathbf{H}}_{a,k}^H + \tilde{\mathbf{x}}_k \tilde{\mathbf{y}}_{a,k}^H \frac{\mathbb{E}_u[u]}{\sigma_a^2}\right)\right]^H, \quad (25)$$

$$\mathbf{\Omega}_{\mathbf{H}_{a,k}} = \left[\frac{1}{\sigma_\epsilon^2} \mathbf{I} + \tilde{\mathbf{x}}_k \tilde{\mathbf{x}}_k^H \frac{\mathbb{E}_u[u]}{\sigma_a^2}\right]^{-1}. \quad (26)$$

$q(u)$ on the other hand, can be approximated to $\mathcal{G}\left(\frac{v+2N}{2}, \frac{v+C}{2}\right)$, with

$$C = \left(\tilde{\mathbf{y}}_{a,k} - \mathbb{E}_{\mathbf{H}_{a,k}}[q(\mathbf{H}_{a,k})] \tilde{\mathbf{x}}_k\right)^H \left(\tilde{\mathbf{y}}_{a,k} - \mathbb{E}_{\mathbf{H}_{a,k}}[q(\mathbf{H}_{a,k})] \tilde{\mathbf{x}}_k\right) \\ + \tilde{\mathbf{x}}_k^H [\mathbf{\Omega}_{\mathbf{H}_{a,k}} M_{\text{AP}}] \tilde{\mathbf{x}}_k \frac{1}{\sigma_a^2}. \quad (27)$$

2) *M-step*: For the variational M-step, \mathcal{F} is maximized in terms of ϑ with fixed $q(\mathbf{h}_{a,k})$. Again, after every $(a+1)$ th iteration, ϑ^{a+1} is obtained by

$$\vartheta^{a+1} = \arg \max_{\vartheta} \mathcal{F}_{\tilde{\mathbf{y}}_{a,k}}(q^{a+1}, \vartheta). \quad (28)$$

Given (25) and (26), and after some mathematical manipulations, $\mathcal{F}_{\tilde{\mathbf{y}}_{a,k}}(q^{a+1}, \vartheta)$ can be written as $\sigma_a^2 C$. Thus, the estimated transmitted interference signal, $\hat{\mathbf{x}}_k$ can be recovered by minimizing $\mathcal{F}_{\tilde{\mathbf{y}}_{a,k}}(q^{a+1}, \vartheta)$. However, to facilitate the analysis, a Choleski decomposition may be applied on $\mathbf{\Omega}_{\mathbf{H}_{a,k}} M_{\text{AP}} = \mathbf{V}_{\mathbf{H}}^\top \mathbf{V}_{\mathbf{H}}$, and $\hat{\mathbf{x}}_k$ is obtained via the following optimization

$$\hat{\mathbf{x}}_k = \min\left(\|\tilde{\mathbf{y}}_{a,k} - \mathbb{E}_{\mathbf{H}_{a,k}}[q(\mathbf{H}_{a,k})] \tilde{\mathbf{x}}_k\|^2 + \|\mathbf{V}_{\mathbf{H}} \tilde{\mathbf{x}}_k\|^2\right). \quad (29)$$

The EM implementation is described in Algorithm 2.

In Algorithm 2, $\hat{\mathbf{x}}_k^{\text{ZF}}$ is computed via a zero-forcing (ZF) detector as

$$\hat{\mathbf{x}}_k^{\text{ZF}} = (\hat{\mathbf{H}}_{a,k}^H \hat{\mathbf{H}}_{a,k})^{-1} \hat{\mathbf{H}}_{a,k}^H \mathbf{y}_{a,k}. \quad (30)$$

Accordingly, after $\hat{\mathbf{x}}_k$ is obtained, its covariance matrix is computed as $\mathbf{R}_{\hat{\mathbf{x}}_k} = \hat{\mathbf{x}}_k \hat{\mathbf{x}}_k^H$, and the estimated beampattern for the k th transmitter AP is designed as

$$\hat{\mathbf{B}}_k = \mathbf{a}^H(\theta_z) \mathbf{R}_{\hat{\mathbf{x}}_k} \mathbf{a}(\theta_z), \forall k, \quad (31)$$

As illustrated in Fig. 2, the adversary consider the maximum angle from $\hat{\mathbf{B}}_k$ as the estimated direction of the beam of

Algorithm 2 EM Algorithm

```

1: Initialize:
    $\mathbb{E}_{\mathbf{H}_{a,k}}^{(0)}[q(\mathbf{H}_{a,k})] \leftarrow \hat{\mathbf{H}}_{a,k}; \hat{\mathbf{x}}_k^{(0)} \leftarrow \hat{\mathbf{x}}_k^{\text{ZF}}; a \leftarrow 0$ 
2: while convergence = 0 do
3:   Calculate  $q^{(a+1)}(u)$  and  $\mathbb{E}_u[u]^{(a+1)}$ .
4:   Update  $\mathbb{E}_{\mathbf{H}_{a,k}}^{(a+1)}$  according to (25), and  $\Omega_{\mathbf{H}}^{(a+1)}$  as in (26).
5:   Do the Cholesky decomposition:  $\Omega_{\mathbf{H}}^{(a+1)} \mathbf{M}_{\text{AP}} = \mathbf{V}_{\mathbf{H}}^{(a+1)T} \mathbf{V}_{\mathbf{H}}^{(a+1)}$ .
6:   Solve the minimization problem in (29) to achieve  $\hat{\mathbf{x}}_k^{(a+1)}$  given
      $\mathbf{V}_{\mathbf{H}}^{(a+1)}$  and  $\mathbb{E}_{\mathbf{H}_{a,k}}^{(a+1)}$ .
7:   if  $\|\hat{\mathbf{x}}_k^a - \hat{\mathbf{x}}_k^{a-1}\| \leq \text{cov}$  then
8:     convergence = 1
9:   else
10:     $a \leftarrow a + 1$ ;
11:    Return to Step 3.
12:   end if
13: end while
14: return  $\hat{\mathbf{x}}_k^a$ .

```

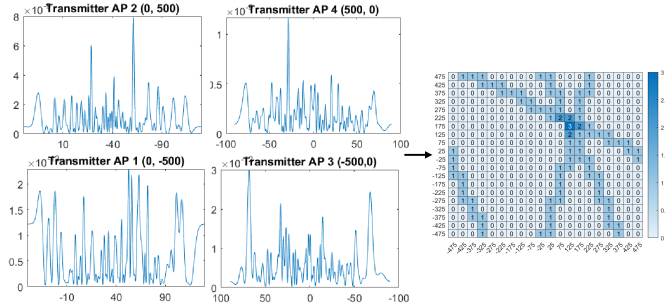


Fig. 2: A schematic of the process to compute the location of the target.

AP k to the target and defines a line of search inscribed in a square search area, having as many lines as number of transmitter APs. Next, the adversary divides the search area in cells of same size and verifies which of them are crossed by the computed direction lines. At the end, the cell crossed by the highest number of lines is set as the estimated position for the target. In case more than one cell contains the maximum number of crossing lines, the estimated position is selected randomly among the cells with maximum value. Thus, the probability of detection for an observation q is given by

$$P_{D,q} = \begin{cases} 1 & \text{if } \hat{Pos}_{t,q} = Pos_t \\ 0 & \text{otherwise,} \end{cases} \quad (32)$$

where Pos_t and $\hat{Pos}_{t,q}$ are, respectively, the true and estimated position of the target. Hence the probability of detection for the total number of observations Q is given by $P_D = \sum_{q=1}^Q P_{D,q}/Q$.

V. NUMERICAL RESULTS AND DISCUSSIONS

For the numerical results, the search area is assumed to have $1000 \text{ m} \times 1000 \text{ m}$, with cells of $50 \text{ m} \times 50 \text{ m}$ and the coordinate $(0,0)$ positioned at the center of the search area. It is considered $N_{\text{Tx}}=8$ transmitter APs serving $N_{\text{Ue}}=4$ UEs with $M_{\text{Ue}}=8$ antennas each. It is also assumed $N_{\text{Rx}}=4$ sensing receiver APs, and both transmitter and receiver APs are equipped with $M_{\text{AP}}=64$ antennas. The noise variance for each user, σ_i^2 , the communication SINR threshold, Γ , and

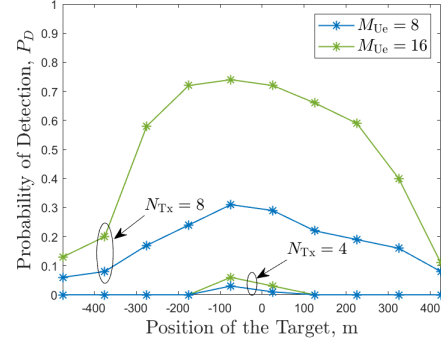


Fig. 3: Probability of Detection, P_D vs. the position of the target for $M_{\text{Ue}}=8, 16$ and $N_{\text{Tx}}=4, 8$.

the maximum transmit power per AP, P_T are respectively set as -94 dBm , 3 dBm and 50 dBm . The carrier frequency is $\lambda_c=1.9 \text{ GHz}$, and the variance of the RCS is $\sigma_{r,k}^2=10 \text{ dBsm}$. In addition, the average channel gains of the communication links are assumed to be determined by the pathloss, i.e., $\Omega_{i,k}=d_{i,k}^{-\varphi}$, where $d_{i,k}$ is the distance between the k th transmitter AP and UE i , and the path-loss exponent is set as $\varphi=3$. For algorithm 1, the error tolerance ϵ is set as 0.1 and $p_{\text{max}}=10$ proved to render a sufficient number of iterations. Moreover, $\mathbf{W}^{(0)}$ and $\mathbf{u}_i(0)$ are chosen randomly. For algorithm 2, the variance of the channel estimation error is $\sigma_\varepsilon^2=10 \text{ dBm}$ and $\text{cov}=10^{-5}$. P_D is computed over $Q=100$ channel realizations, and unless specified otherwise the coordinates of the target is $(-75, 75)$, the receiver APs are at $(250, 250)$, $(-250, -250)$, $(-250, 250)$ and $(250, -250)$. The UEs are positioned at $(300, 300)$, $(-300, -300)$, $(-300, 300)$ and $(300, -300)$, where the first one is considered as the adversary. Finally, the eight transmitter APs are at $(-500, -500)$, $(500, 500)$, $(-500, 500)$, $(500, -500)$, $(0, -500)$, $(0, 500)$, $(-500, 0)$ and $(500, 0)$.

Fig. 3 illustrates P_D vs. the position of the target for $M_{\text{Ue}}=8, 16$ and $N_{\text{Tx}}=4, 8$. For this figure, the target's position is varied along the main diagonal of the search area, with the label of Fig. 3 indicating the variation along the x-axis. Also, the coordinates of transmitter APs for the case with $N_{\text{Tx}}=4$ are $(0, -500)$, $(0, 500)$, $(-500, 0)$ and $(500, 0)$. Note that larger number of antennas at UEs increases the probability of detection by the adversary, as expected. Although the increase is noticeably more pronounced when the number of transmitter APs is also larger, as it increases the possibility that a bigger number of estimated direction lines converges to the cell that contains the target. Moreover, notice that the maximum P_D for all cases occurs when the target is positioned closer to the center of the search area, which is also the closer point to the adversary location. In that case, the interference from the sensing signal at the adversary is higher, thus allowing for a better estimation from the EM algorithm. For the worst case, with $N_{\text{Tx}}=8$ and $M_{\text{Ue}}=16$, it leads to a P_D higher than 0.7 which highlights the risk for the target's location privacy.

In Fig. 4, P_D is evaluated for different sizes of cells

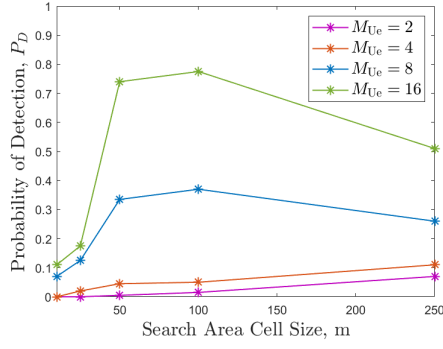


Fig. 4: Probability of Detection, P_D vs. the search area cell size for $M_{UE}=2, 4, 8, 16$.

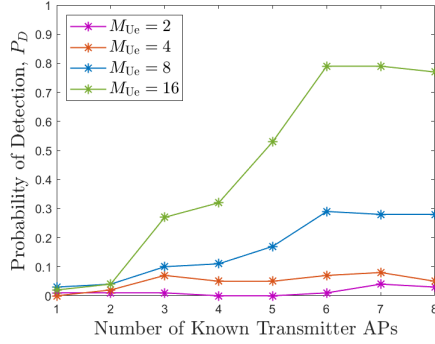


Fig. 5: Probability of Detection, P_D vs. the number of known transmitter APs for $M_{UE}=2, 4, 8, 16$.

and different values of the number of antennas at the UEs, $M_{UE}=2, 4, 8, 16$. Validating the results observed in the previous figure, by increasing the number of antennas at the UEs, P_D also increases. Note that for cases $M_{UE}=8$ and $M_{UE}=16$, there is a decrease on P_D when the cell size is bigger than 100 m. It can be explained by the fact that there are fewer cells within the search area as the cell size increases, thus more cells might contain the maximum number of crossing lines, which reduces the probability that the chosen estimate position be the correct one. Even though, the P_D remains relatively high, with the adversary identifying the correct cell in more than 50% of the cases.

Fig. 5 illustrates P_D vs. the number of known transmitter APs position from the adversary for $M_{UE}=2, 4, 8, 16$. For this figure, we consider that the adversary receives data from all transmitter APs, but might not be capable to identify the location of all them. Note that, for $M_{UE}=8, 16$, with the knowledge of 6 transmitter APs, the adversary is already capable to achieve the maximum P_D for both values of M_{UE} . Also, even with the position information of fewer APs, the adversary can still correctly detect the target in several opportunities.

VI. CONCLUSIONS

In this paper, the capability of an UE, acting as adversary, to infer the position of a target in a multi-static sensing-centric ISAC system was investigated. For the adversary model, an EM algorithm was proposed to obtain an estimation of the

transmitted signal, which was used to create replicas of the transmit beampattern of each transmitter AP. From the results, we showed that as more APs are deployed than transmitters, the adversary is capable to successfully identify the target location in a reasonable number of cases. Different from the mono-static scenario, where the adversary is capable to infer the angular position of the target, the multi-static sensing-centric scenario showed to be more critical in terms of privacy, since the adversary is capable of, with some accuracy, identify the exact location of the target. These threat becomes even more critical as the network becomes denser.

ACKNOWLEDGEMENT

This work has been supported by Academy of Finland, 6G Flagship program (Grant 346208) and FAITH Project (Grant 334280). Codes to reproduce results are available at: <https://github.com/isabella-gomes/Globecom2023>

REFERENCES

- [1] F. Liu and Et. al., "Integrated sensing and communications: Toward dual-functional wireless networks for 6G and beyond," *IEEE Journal on Sel. Areas in Commun.*, vol. 40, no. 6, pp. 1728–1767, 2022.
- [2] Z. Behdad and Et. al., "Multi-static target detection and power allocation for integrated sensing and communication in cell-free massive MIMO," *arXiv preprint arXiv:2305.12523*, 2023.
- [3] Y. Huang, Y. Fang, X. Li, and J. Xu, "Coordinated power control for network integrated sensing and communication," *IEEE Trans. on Veh. Technol.*, vol. 71, no. 12, pp. 13 361–13 365, 2022.
- [4] X. Liu and Et. al., "Joint transmit beamforming for multiuser MIMO communications and mimo radar," *IEEE Trans. on Sig. Process.*, vol. 68, pp. 3929–3944, 2020.
- [5] U. Demirhan and A. Alkhateeb, "Cell-free ISAC MIMO systems: Joint sensing and communication beamforming," *arXiv preprint arXiv:2301.11328*, 2023.
- [6] N. Su, F. Liu, and C. Masouros, "Secure radar-communication systems with malicious targets: Integrating radar, communications and jamming functionalities," *IEEE Trans. on Wireless Commun.*, vol. 20, no. 1, pp. 83–95, 2021.
- [7] —, "Sensing-assisted physical layer security," in *WSA'1&' SCC 2023; 26th International ITG Workshop on Smart Antennas and 13th Conference on Systems, Communications, and Coding*, 2023, pp. 1–6.
- [8] Z. Ren, L. Qiu, and J. Xu, "Optimal transmit beamforming for secrecy integrated sensing and communication," in *ICC 2022-IEEE International Conference on Communications*. IEEE, 2022, pp. 5555–5560.
- [9] I. W. G. da Silva, D. P. Osorio, and M. Juntti, "Privacy performance of MIMO dual-functional radar-communications with internal adversary," *arXiv preprint arXiv:2302.06253*, 2023.
- [10] I. W. G. da Silva, E. E. B. Olivo, M. Katz, and D. P. M. Osorio, "Secure precoding and user association for multiuser hybrid RF/VLC systems," *TechRxiv preprint:10.36227/techrxiv.20412177.v2*, 2023.
- [11] Q. Shi, M. Razaviyayn, M. Hong, and Z.-Q. Luo, "SINR constrained beamforming for a MIMO multi-user downlink system: Algorithms and convergence analysis," *IEEE Trans. on Signal Proc.*, vol. 64, no. 11, pp. 2920–2933, 2016.
- [12] M. Haugh, "The EM algorithm," http://www.columbia.edu/~mh2078/MachineLearningORFE/EM_Algorithm.pdf, 2015.
- [13] Y. Zhang, J. Sun, J. Xue, G. Y. Li, and Z. Xu, "Deep expectation-maximization for joint MIMO channel estimation and signal detection," *IEEE Trans. on Sig. Process.*, vol. 70, pp. 4483–4497, 2022.